

Cortical Bone Water Changes in Ovariectomized Rats During the Early Postoperative Period: Objective Evaluation Using Sweep Imaging With Fourier Transform

Tsuyoshi Sukenari, MD,¹ Motoyuki Horii, MD,¹ Kazuya Ikoma, MD, PhD,^{1*} Masamitsu Kido, MD, PhD,¹ Shigeki Hayashi, MD,¹ Yusuke Hara, MD,¹ Tetsuro Yamasaki, MD,¹ Ken-ichi Matsuda, PhD,² Mitsuhiro Kawata, MD, PhD,² and Toshikazu Kubo, MD, PhD¹

Purpose: To evaluate the cortical bone signal-to-noise ratio (SNR) in ovariectomized (OVX) rats during the early postoperative period as a method to measure bone quality using the sweep imaging with Fourier transform (SWIFT) technique.

Materials and Methods: Twelve-week-old female Sprague–Dawley rats ($n = 64$) were divided into sham and OVX groups. Preoperative tetracycline was immediately administered subcutaneously to distinguish new cortical bone area, and tibial samples were collected at 2, 4, 8, and 12 weeks postoperatively. Magnetic resonance imaging (MRI) was performed using proton density-weighted imaging (PDWI) and SWIFT to obtain cross-sectional images of the tibial diaphysis. The cortical bone SNR was calculated. Bone histomorphometry was performed.

Results: Histomorphometry findings showed that the new bone area was significantly greater at 8 and 12 weeks postoperatively in the OVX group ($P < 0.05$) while the porosity area decreased gradually in both groups ($P < 0.001$). The difference of SNR receiving PDWI did not reach statistical significance ($P = 0.057$). The SWIFT technique showed that the SNR was significantly higher at 8 and 12 weeks postoperatively in the OVX group ($P < 0.05$) and was correlated with the new bone area ($R^2 = 0.430$).

Conclusion: The SWIFT findings suggest that the SWIFT technique may depict early changes in cortical bone quality.

Key Words: bone water; cortical bone; osteoporosis; ovariectomy; sweep imaging with Fourier transform

J. Magn. Reson. Imaging 2014;00:000–000.
© 2014 Wiley Periodicals, Inc.

OSTEOPOROSIS is defined by decreased bone strength and increased fracture risk (1). Bone strength is reflected in bone density and quality. Bone quality is affected by bone architecture, turnover, accumulated damage, and mineralization (1). Postmenopausal osteoporosis is the most common form of osteoporosis. Ovariectomized rats are used generally in the research of postmenopausal osteoporotic models (2). The menopause-associated decrease in estrogen concentration increases the bone resorption rate. This ultimately leads to osteoporosis (3,4), increases risks of bone fracture and death (5), and deteriorates quality-of-life (QOL) (6).

Secondary osteoporosis caused by diabetes (7) and glucocorticoid therapy (8) also degrades bone quality by affecting collagen cross-linking (9); as a result, bone fractures can occur even in people with a high bone mineral density (BMD), highlighting the importance of assessing not only BMD, but also bone quality.

Cortical bone is also important to maintain bone strength (10). To assess cortical bone quality, cortical bone water is measured by magnetic resonance imaging (MRI) (11). Cortical bone consists of ~65% mineral, ~10% organic matrix, and ~25% water (12,13). Some bone water resides within the pore spaces, which include the lacunocanalicular system and blood vessels such as the Haversian canal and Volkmann canal (14–17). The remaining bone water binds to the matrix substrate and collagen, and binds tightly to crystalline components such as hydroxyapatite.

In recent years, ultrashort echo time (UTE) imaging (13) and sweep imaging with Fourier transform (SWIFT) (18,19) have been used to image tissues such as bone with an extremely short T_2 relaxation time. In the

¹Department of Orthopaedics, Graduate School of Medical Science, Kyoto Prefectural University of Medicine, Kyoto, Japan.

²Department of Anatomy and Neurobiology, Graduate School of Medical Science, Kyoto Prefectural University of Medicine, Kyoto, Japan.

*Address reprint requests to: K.I., Department of Orthopaedics, Graduate School of Medical Science, Kyoto Prefectural University of Medicine, 465 Kajii-cho, Kawaramachi-Hirokoji, Kamigyo-ku, Kyoto, Japan. E-mail: kazuya@koto.kpu-m.ac.jp

Received July 19, 2014; Accepted September 8, 2014.

DOI 10.1002/jmri.24765

View this article online at wileyonlinelibrary.com.

SWIFT technique, the TE is set to nearly 0, and excitation and signal acquisition are performed at almost the same time; this enables signal detection and imaging of tissues with extremely short T_2 relaxation times (18). The SWIFT technique also enables detection of bound water with an extremely short T_2 relaxation time and may distinguish changes in cortical bone quality.

The purpose of this study was to evaluate the tibial cortical bone signal-to-noise ratio (SNR) in ovariectomized (OVX) rats during the early postoperative period as a method to measure bone quality by conducting MRI using the SWIFT technique.

MATERIALS AND METHODS

Animal Model

Twelve-week-old female Sprague–Dawley (SD) rats ($n = 64$) (Shimizu Laboratory Supplies, Kyoto, Japan) were studied. The rats were housed in our institution's animal facility in accordance with the guidelines of the *Guide for the Care and Use of Laboratory Animals* published by the National Institutes of Health. The facility was maintained at a 23–24°C room temperature on a 12-hour light/dark schedule, and the subjects had free access to food and water. The rats were randomized into sham or OVX experimental groups. This study was approved by our Institutional Review Board for animal experiments.

The sham operation and ovariectomy were performed under sterile conditions. All rats were anesthetized with 1.5% isoflurane. In both experimental groups, an abdominal incision was made and the ovaries were identified; the ovaries were removed from the OVX subjects but left intact in the sham subjects.

The animals were sacrificed using intraperitoneal sodium pentobarbital at 2, 4, 8, and 12 weeks postoperatively. The OVX rats had a higher body weight because of estrogen deficiency, compared to the sham rats, a finding that has been reported previously (20–22). Successful OVX was confirmed at necropsy by uterine horn atrophy. The tibias were extracted as a single specimen, placed in a 1.5-cm-diameter columnar container, and immersed in a fluorine-based inert liquid (Fluorinert FC-3283; Sumitomo 3M, Tokyo, Japan) to reduce potential imaging artifacts.

MRI

Imaging was performed on a small bore MRI unit (Varian MRI System 7.04T; Agilent Technologies, Palo Alto, CA) using a transmit/receive surface coil (3×3 cm diameter). The specimen container was set on the surface coil center to avoid radiofrequency (RF) variation. The specimens were placed in the same direction to maintain a specific flip angle (FA).

The tibias were imaged using the SWIFT technique as follows: repetition time (TR), 12.5 msec; FA, 25°; matrix, $256 \times 256 \times 256$; views, 8192; average, 1; field of view (FOV), $40 \times 240 \times 40$ mm³; resolution, $0.156 \times 0.938 \times 0.156$ mm³; bandwidth, 62.5 kHz; readout times, 4.096 msec; and total scan time, 27 minutes 25 seconds. To investigate conventional MR

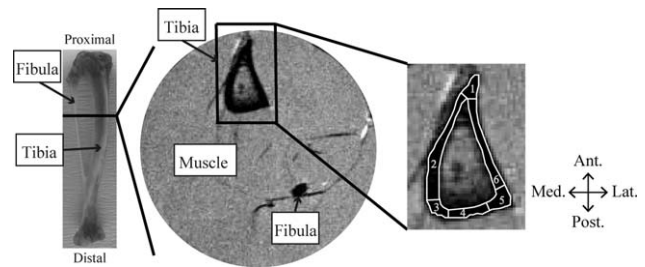


Figure 1. Setting ROI surrounded by the white line. Six ROIs, including all areas of the cortical bone, are set in the cortical bone in the diaphysis of the tibia with the transected image (proton density-weighted image). Ant., Anterior; Lat., Lateral; Med., Medial; Post., Posterior.

images, the fast spin echo method was performed to acquire the proton density-weighted image (PDWI) as follows: TR, 2000 msec; TE, 9.54 msec; echo train length, 4; average, 1; matrix, 256×256 ; FOV, 40×40 mm²; resolution, 0.156×0.156 mm²; axial slice, 30; slice thickness, 1 mm; gap, 0 mm with interleave; bandwidth, 100 kHz; readout times, 2.56 msec; and total scan time, 4 minutes 20 seconds. The first slice was set at the most proximal side of the tibia. Six regions of interest (ROIs), including all areas of the cortical bone, were set in the cortical bone in the proximal one-third of the tibial cortical bone with the same transected image (Fig. 1). The sizes of the ROIs were anterior, 0.55 ± 0.13 cm² (Fig. 1-1 in cortical bone); medial, 0.75 ± 0.17 cm² (Fig. 1-2); posteromedial, 0.62 ± 0.12 cm² (Fig. 1-3); posterior, 0.58 ± 0.14 cm² (Fig. 1-4); posterolateral, 0.72 ± 0.13 cm² (Fig. 1-5); lateral, 0.72 ± 0.15 cm² (Fig. 1-6); and total, 3.93 ± 0.39 cm². The signal intensity (SI) of the ROI was measured and averaged. The SNR, defined as the ratio between the mean SI to the background noise standard deviation, was calculated (13). The ROI to measure the background noise standard deviation was placed in an artifact-free position as large as possible. The SI and the background noise standard deviation were measured using an MRI unit software (VnmrJ v. 3.1; Agilent Technologies).

BMD Measurement

The tibias were fixed in 70% ethanol immediately after performing the MRI. The surrounding soft tissues were detached and the tibial BMD was measured using dual-energy X-ray absorptiometry (DEXA) (DCS-600EX-R; Aloka, Tokyo, Japan).

μ CT Analyses

The tibias were imaged using microcomputed tomography (μ CT) (micro focus 2D/3D, ScanXmate-E090S40; Comscantecno, Kanagawa, Japan) under the following conditions: voltage, 60 kV; electric current, 85 μ A; and voxel size, 37.5 μ m. Three-dimensional reconstructions were created using commercial image reconstruction software (FanCT version 1.3; Comscantecno). The 200- μ m-thick transected tibial images were prepared at the location identical to

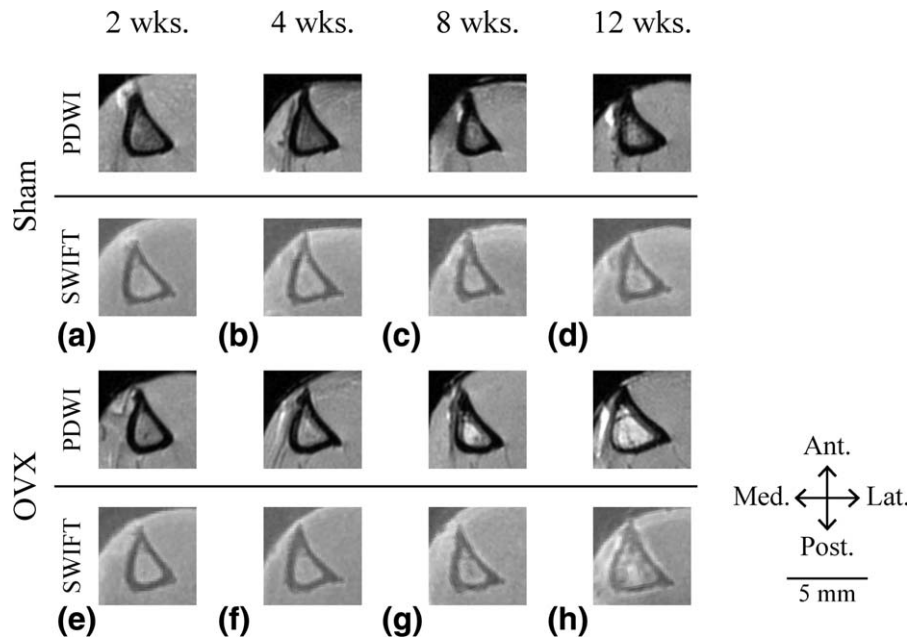


Figure 2. Representative PDWI images (top row) and SWIFT images (bottom row) in sham rats (a–d) and OVX rats (e–h) at 2, 4, 8, and 12 weeks postoperatively. The SI of the cortical bone is measured from these images. Ant., Anterior; Lat., Lateral; Med., Medial; Post., Posterior.

previous MRI images. The cortical BMD, mean cortical width, and marrow area were measured using commercial image analysis software (TRI/3D-BON; RATOC System Engineering, Tokyo, Japan).

Bone Histomorphometry

Preoperative tetracycline hydrochloride (Sigma-Aldrich, St. Louis, MO) was immediately administered dorsal subcutaneously to distinguish new cortical bone area. Forty specimens that were not decalcified were randomly selected at 2, 4, 8, and 12 weeks postoperatively. The specimens were stained with Villanueva bone stain, embedded in methyl methacrylate, and prepared at a location closely matched to that using the MRI.

The cortical bone histomorphometric characteristics were measured according to Parfitt's method (23) as follows: porosity area (Po. Ar), cortical area (Ct. Ar), and new bone area (New B. Ar). Pores were designated as the Po. Ar, except for osteocytic lacunae within cortical bone, and examined under natural light and 100 \times magnification. The Ct. Ar was measured at 200 \times magnification, as was the New B. Ar from cortical bone surface to tetracycline labeled under fluorescent light and 200 \times magnification. The secondary parameters, including Po. Ar/Ct. Ar (%), and New B. Ar/Ct. Ar (%), were calculated as a ratio to each measured cortical area.

Statistical Analyses

Measurements were expressed as the mean \pm standard deviation. Two-way analysis of variance (ANOVA) was used to analyze BMD, μ CT measurements (cortical BMD, cortical width, and marrow area), the SNRs for both groups during PDWI and SWIFT, and bone histomorphometry (Ct. Ar, Po. Ar/Ct. Ar, and New B. Ar/Ct. Ar) with group (sham or OVX) and postoperative week (2, 4, 8, or 12 weeks) as between-subject factors; Tukey's post-hoc test was performed for multiple comparisons. Correlations between SNRs at

SWIFT and cortical BMD or New B. Ar/Ct. Ar (%) were determined using Pearson's correlation test. A value of $P < 0.05$ was considered statistically significant. Statistical analyses were conducted using SPSS (v. 21.0 for Windows; IBM, Chicago, IL).

RESULTS

MRI

The cortical bone SNRs within the OVX group were compared to the sham group under either PDWI or SWIFT (Fig. 2, 3). The difference of SNR between the sham and OVX groups receiving PDWI did not quite reach statistical significance ($F_{(1,56)} = 3.79$, $P = 0.057$, 95% confidence interval for difference -0.579 to 0.008), although the SNR of the OVX-PDWI rats tended to be higher than that of the sham-PDWI rats (Fig. 3a). In rats imaged by SWIFT, the SNR in the OVX group was significantly higher than that in the sham group at 8 and 12 weeks postoperatively ($P = 0.016$ and $P = 0.019$, respectively) (Fig. 3b).

BMD Measurement

The tibial BMD was compared between the OVX and sham groups. BMD was lower in the OVX group than in the sham group at all points evaluated ($F_{(1,56)} = 26.77$, $P < 0.001$) (Fig. 4a).

μ CT Analyses

The cortical BMD was lower in the OVX than in the sham group at all points evaluated ($F_{(1,56)} = 14.74$, $P < 0.001$) (Fig. 4b). The cortical BMD was positively, though weakly, correlated ($R^2 = 0.066$) with the cortical bone SNRs at SWIFT ($P = 0.037$) (Fig. 4c). The cortical width in OVX subjects was significantly thicker than that in sham subjects at 2 weeks postoperatively ($P = 0.006$) and significantly thinner than that in

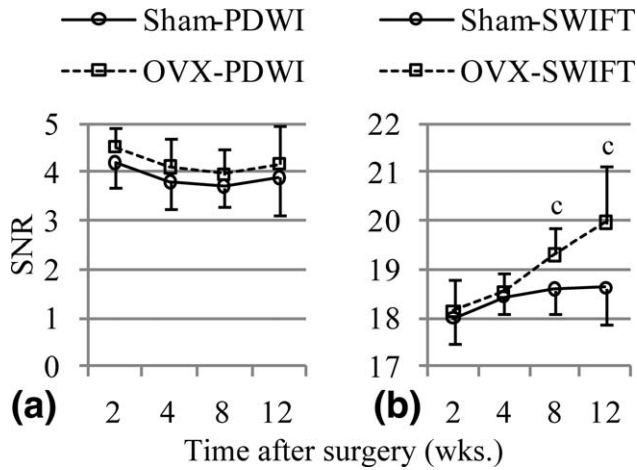


Figure 3. SNR in the tibial cortical bone in PDWI (a) and SWIFT (b). The SI of the ROI in the cortical bone was measured and averaged. The SNR, defined as the ratio between the mean SI to the background noise standard deviation, was calculated. Values are expressed as the mean \pm standard deviation. a: $P < 0.001$, b: $P < 0.01$, and c: $P < 0.05$ vs. the sham group.

sham subjects at 12 weeks postoperatively ($P = 0.012$) (Fig. 4d). The marrow area was significantly larger in OVX subjects than in sham subjects at only 12 weeks postoperatively ($P = 0.001$) (Fig. 4e).

Bone Histomorphometry

The Po. Ar increased in the OVX specimens, compared to the sham specimens under fluorescent light visually.

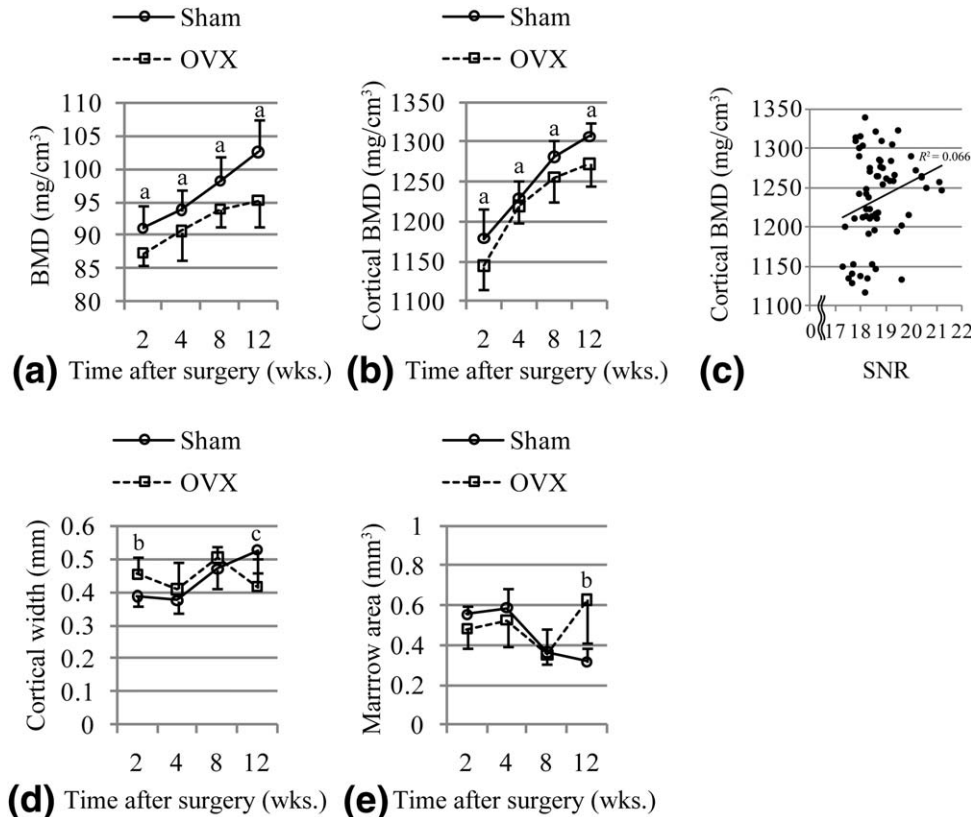


Figure 4. The tibial BMD (a) and cortical bone μ CT measuring cortical BMD (b), cortical width (d), and marrow area (e). Values are expressed as the mean \pm standard deviation. a: $P < 0.001$, b: $P < 0.01$, c: $P < 0.05$ vs. the sham group. The SNRs using SWIFT is correlated significantly with cortical BMD ($P = 0.037$), but the correlation is weakly positive ($R^2 = 0.066$) (c).

The marrow area was enlarged and the cortical width reduced in the OVX group at 12 weeks postoperatively (Fig. 5a-h). Under fluorescent light, tetracycline labeling was present on the endosteal perimeter, particularly on the posterior to lateral margins and anterior to medial periosteal margins. The New B. Ar is shown in Fig. 5i. Cortical bone drifted toward the posterolateral side. The Ct. Ar did not differ significantly between the sham and OVX groups (Fig. 6a). The Po. Ar/Ct. Ar was larger in the OVX group than in the sham group at all weeks postoperatively ($F_{(1,32)} = 18.72$, $P < 0.001$) and decreased in a time-dependent manner in both groups ($F_{(3,32)} = 22.41$, $P < 0.001$) (Fig. 6b). The New B. Ar/Ct. Ar in OVX specimens was significantly smaller than that in sham specimens at 8 and 12 weeks postoperatively ($P = 0.004$ and $P = 0.022$, respectively) (Fig. 6c). The New B. Ar/Ct. Ar was correlated significantly with the cortical bone SNRs at SWIFT ($P < 0.001$), and the relationship was strong, with a positive correlation coefficient ($R^2 = 0.430$) (Fig. 6d).

P -values of two-way ANOVA for results are shown in Table 1.

DISCUSSION

In OVX rats, bone turnover at the proximal tibia is reportedly faster than at the lumbar spine and proximal femur (24–26), and there is significant cancellous bone loss observed histologically in the proximal tibia at 2 weeks postoperatively (24). In this study, DEXA showed that beginning 2 weeks postoperatively, the tibial BMD decreased significantly in the OVX group compared to the sham group, which was consistent

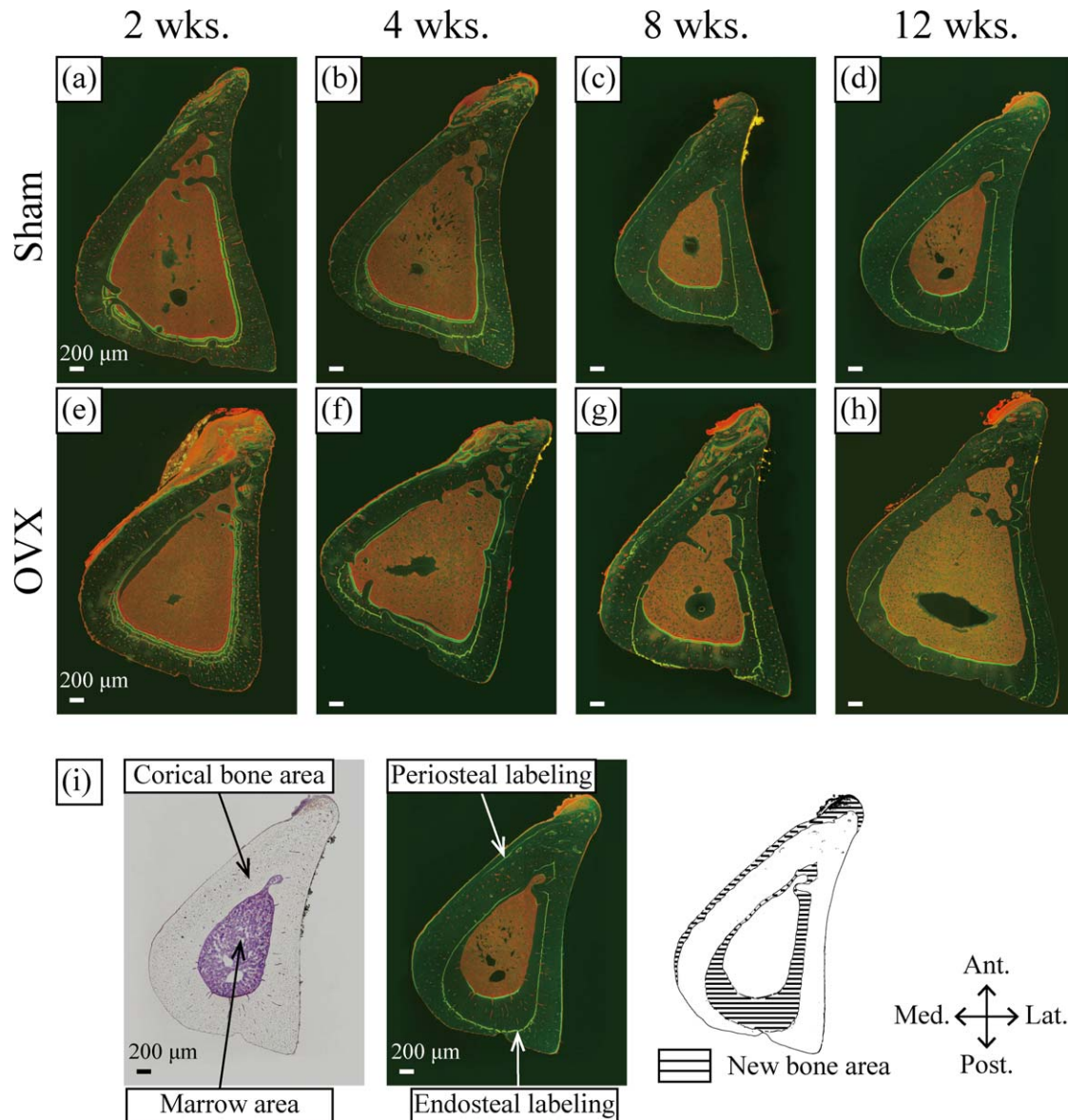


Figure 5. Representative images of histological tibial transections under fluorescent light in the sham rats (a–d) and OVX rats (e–h) at 2, 4, 8, and 12 weeks postoperatively. Porosity is increased in the OVX group compared to the sham group (orange areas in the cortical bone). Representative image of sham group at 12 weeks postoperatively (i). Histological image under natural light is shown (left). Tetracycline labeling lined by yellow is observed at the endosteal and periosteal sides under fluorescent light (center). The new bone area is shown by the area of broken lines (right). Ant., Anterior; Lat., Lateral; Med., Medial; Post., Posterior.

with previous reports. However, DEXA measures BMD changes including both the cancellous and cortical bone and therefore distinguishing and measuring each individual component in small animals is difficult. In addition, DEXA enables only 2D projections and does not allow 3D assessments. Previous reports indicate that BMD measurement using DEXA alone does not allow the evaluation of potential fracture risks (27,28); bone quality and cortical bone must also be evaluated.

Previous reports using μ CT revealed that the cortical BMD did not change as significantly as the cancellous bone during the early OVX postoperative period; several reports have actually shown a low cortical BMD (29,30). Samnegard et al (31) observed that in 3.5-month-old SD rats, the femoral diaphyseal BMD

decreased significantly 11 weeks after OVX. Although the cortical bone BMD in this study did not differ markedly from previous reports, there were significant differences during the early postoperative period. Previous reports reveal differences in the bone turnover rates between the proximal and distal tibial regions in OVX rats (32). In our study, a slightly proximal location with a larger muscle mass was targeted to achieve improved MRI contrast, which may have influenced the present findings. The increased porosity area observed in the OVX group at each week postoperatively may have also influenced the findings. An enlarged marrow area and reduced cortical width have both been previously reported 3 months following OVX (29,33), which is consistent with our observations. The enlarged marrow area and decreased cortical width

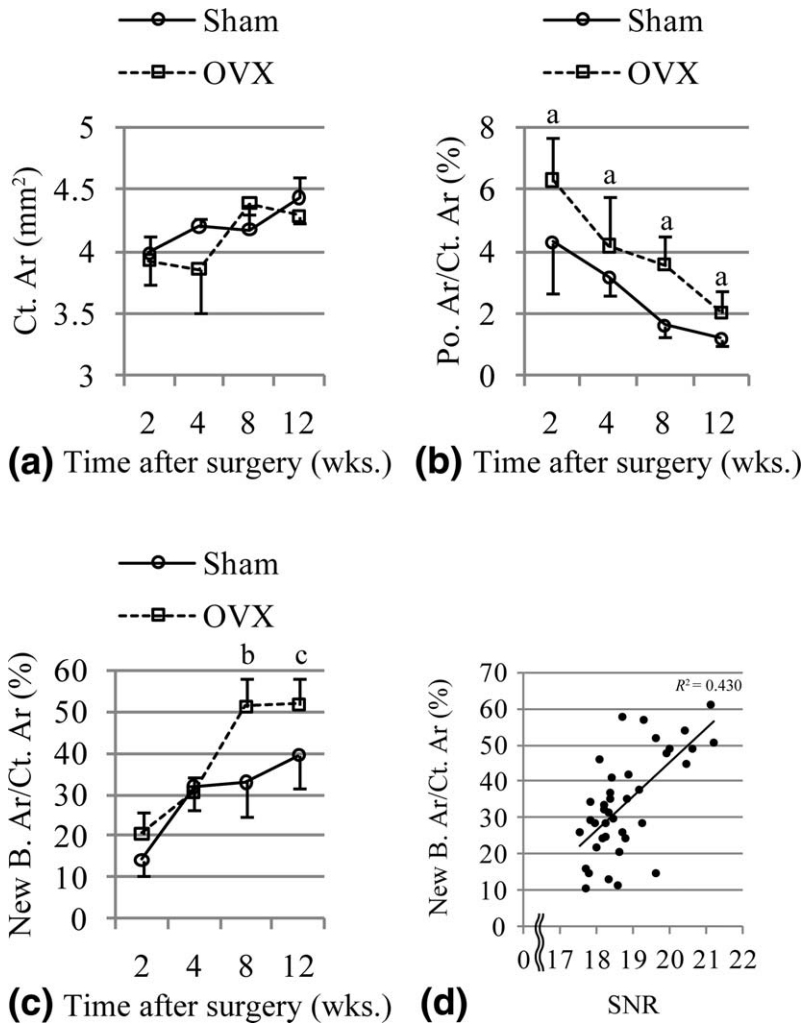


Figure 6. Tibial cortical bone histomorphometry. Cortical area (Ct. Ar) (a), porosity area/cortical area (Po. Ar/Ct. Ar) (b), and new bone area/cortical area (New B. Ar/Ct. Ar) (c). Values are expressed as the mean \pm standard deviation. a: $P < 0.001$, b: $P < 0.01$, and c: $P < 0.05$ vs. the sham group. The cortical bone SNRs of the SWIFT data correlate significantly with the New B. Ar/Ct. Ar ($P < 0.001$), and the relationship is strongly positive ($R^2 = 0.430$) (d).

suggest that bone resorption was enhanced. The cortical bone began changing during the initial postoperative period, and bone resorption accelerated, particularly beyond 8 weeks postoperatively.

Du et al (17) measured signals from human tibial cortical bone using UTE imaging and reported that only 22.4% was derived from free water fraction, while 77.6% was derived from bound water fraction. This suggests that there is a little free water in the cortical bone. Du et al (17) showed that cortical bone signals obtained using PDWI detected mainly water signals with a millisecond T_2 component. In our study, the absence of any significant difference between the OVX and sham groups in the cortical bone SNR of PDWI suggested that the changes in the millisecond T_2 component were not considerable. The bound water in cortical bone has $\sim 12\text{-}\mu\text{s}$ T_2^* or $\sim 400\text{-}\mu\text{s}$ T_2 (16). The SWIFT technique can depict the free and bound water in cortical bone because the TE is set to a few microseconds (18). Horch et al (16) and Du et al (17) showed that cortical bone water is primarily composed of bound water. When the results for PDWI were also considered, the SNR findings based on the SWIFT technique suggested that bound water

Table 1
 P Values of Two-Way ANOVA for Results

Item	P value of two-way ANOVA		
	Group	Week	Group \times Week
(MRI)			
Cortical bone SNRs			
PDWI	0.057	0.082	0.998
SWIFT	0.001	<0.001	0.041
(DEXA)			
BMD	<0.001	<0.001	0.371
(μCT)			
Cortical BMD	<0.001	<0.001	0.523
Cortical width	0.682	<0.001	<0.001
Marrow area	0.145	<0.001	<0.001
(Histomorphometry)			
Ct. Ar	0.139	<0.001	0.013
Po. Ar/Ct. Ar	<0.001	<0.001	0.496
New B.Ar/Ct. Ar	<0.001	<0.001	0.006

ANOVA, analysis of variance; MRI, magnetic resonance imaging; SNR, signal-to-noise ratio; PDWI, proton density-weighted image; SWIFT, sweep imaging with Fourier transform; DEXA, dual-energy X-ray absorptiometry; BMD, bone mineral density; μCT , microcomputed tomography; Ct. Ar, cortical area; Po.Ar, porosity area; New B. Ar, new bone area.

primarily increased in the cortical bone of the OVX rats, particularly at 8 and 12 weeks postoperatively.

Techawiboonwong et al (11) reported that the amount of human tibial cortical bone water in postmenopausal women was greater than in premenopausal women on UTE imaging because cortical bone porosity increases after menopause. The increased porosity area in OVX rats also supports an increase in cortical bone water content. However, the porosity area decreased with time in both sham and OVX rats, possibly because the SD rats were still growing. The SNR using the SWIFT technique increased with time while the porosity area decreased gradually, suggesting that bound water mainly increased.

The cortical BMD, as well as the SNR as determined using SWIFT data, exhibited only a weak positive correlation; therefore, the cortical bone SNR determined by SWIFT may reflect bone quality that cannot be assessed using BMD alone. The proportion of new bone was significantly greater at 8 and 12 weeks postoperatively in OVX rats, and the new bone area occupied over 50% of all the cortical area at 8 weeks postoperatively. New bone is believed to have high water content. The positive correlation between the new bone area and the cortical bone SNR detected using SWIFT potentially indicates that in OVX rats the early postoperative period is primarily characterized by the increased amount of bound water.

Among the limitations of this study, the specimens were small, and the cortical bone SI was low. Previous reports on SWIFT for bone tissue has only been used for ex vivo specimens (34,35); future establishment of imaging in subjects in vivo is desired. Second, when cortical bone thickness decreases, the influence of the partial volume effect increases, and this is likely to affect the measured SI. In this study, the ROI targeted the cortical bone midline to the greatest extent possible; in future studies, the procedure will need to be conducted in larger animals such as rabbits. Third, the study did not examine the differences between the cortical bone collagen in the OVX and sham groups.

The measurement of the SNR using the SWIFT technique could depict the early cortical bone qualitative changes associated with osteoporosis in humans. In recent years, zero echo time imaging with short and hard pulse excitation has been reported in humans (36). However, the RF power by hard pulse is much higher than by sweep pulse (37). The SWIFT technique may have clinical application because it has less RF peak power, a quiet sequence, and minimal invasion (18,34,37).

In conclusion, this study showed a greater SNR in the tibial cortical bone in OVX rats than in sham rats during the early postoperative period, as detected by MRI using the SWIFT technique. This may reflect a possible increase of bound water in the cortical bone and qualitative changes within the cortical bone in OVX rats. The results for our measurement of cortical bone SNR in OVX rats suggest that MRI using the SWIFT technique may depict early changes in cortical bone quality.

ACKNOWLEDGMENTS

The authors thank Ms. Akemi Ito, a bone histomorphometric specialist, and the staff at Ito Bone Histomorphometry Institute (Niigata, Japan) for their special support. The authors also thank Mr. Nobuhito Nango at RATOC System Engineering (Tokyo, Japan) for advice analyzing μ CT and Dr. Yosuke Yamada at the National Institute of Health and Science for advice on statistical analysis.

REFERENCES

1. NIH Consensus Development Panel on Osteoporosis Prevention, Diagnosis, and Therapy. Osteoporosis prevention, diagnosis, and therapy. *JAMA* 2001;285:785-795.
2. Lelovas PP, Xanthos TT, Thoma SE, Lyritis GP, Dontas IA. The laboratory rat as an animal model for osteoporosis research. *Comp Med* 2008;58:424-430.
3. Cenci S, Weitzmann MN, Roggia C, et al. Estrogen deficiency induces bone loss by enhancing T-cell production of TNF-alpha. *J Clin Invest* 2000;106:1229-1237.
4. Martin TJ, Sims NA. Osteoclast-derived activity in the coupling of bone formation to resorption. *Trends Mol Med* 2005;11:76-81.
5. Nguyen ND, Center JR, Eisman JA, Nguyen TV. Bone loss, weight loss, and weight fluctuation predict mortality risk in elderly men and women. *J Bone Miner Res* 2007;22:1147-1154.
6. Kumamoto K, Nakamura T, Suzuki T, et al. Validation of the Japanese Osteoporosis Quality of Life Questionnaire. *J Bone Miner Metab* 2010;28:1-7.
7. Vestergaard P. Discrepancies in bone mineral density and fracture risk in patients with type 1 and type 2 diabetes—a meta-analysis. *Osteoporos Int* 2007;18:427-444.
8. Kanis JA, Johansson H, Oden A, et al. A meta-analysis of prior corticosteroid use and fracture risk. *J Bone Miner Res* 2004;19:893-899.
9. Saito M, Marumo K. Collagen cross-links as a determinant of bone quality: a possible explanation for bone fragility in aging, osteoporosis, and diabetes mellitus. *Osteoporos Int* 2010;21:195-214.
10. Dickenson RP, Hutton WC, Stott JR. The mechanical properties of bone in osteoporosis. *J Bone Joint Surg Br* 1981;63:233-238.
11. Techawiboonwong A, Song HK, Leonard MB, Wehrli FW. Cortical bone water: in vivo quantification with ultrashort echo-time MR imaging. *Radiology* 2008;248:824-833.
12. Mueller KH, Trias A, Ray RD. Bone density and composition. Age-related and pathological changes in water and mineral content. *J Bone Joint Surg Am* 1966;48:140-148.
13. Du J, Carl M, Bydder M, Takahashi A, Chung CB, Bydder GM. Qualitative and quantitative ultrashort echo time (UTE) imaging of cortical bone. *J Magn Reson* 2010;207:304-311.
14. Timmins PA, Wall JC. Bone water. *Calcif Tissue Res* 1977;23:1-5.
15. Cowin SC. Bone poroelasticity. *J Biomech* 1999;32:217-238.
16. Horch RA, Nyman JS, Gochberg DF, Dortch RD, Does MD. Characterization of 1H NMR signal in human cortical bone for magnetic resonance imaging. *Magn Reson Med* 2010;64:680-687.
17. Du J, Hermida JC, Diaz E, et al. Assessment of cortical bone with clinical and ultrashort echo time sequences. *Magn Reson Med* 2013;70:697-704.
18. Idiyatullin D, Corum C, Park JY, Garwood M. Fast and quiet MRI using a swept radiofrequency. *J Magn Reson* 2006;181:342-349.
19. Idiyatullin D, Corum C, Moeller S, Garwood M. Gapped pulses for frequency-swept MRI. *J Magn Reson* 2008;193:267-273.
20. Gray JM, Wade GN. Food intake, body weight, and adiposity in female rats: actions and interactions of progestins and antiestrogens. *Am J Physiol* 1981;240:E474-E481.
21. Peng ZQ, Vaananen HK, Zhang HX, Tuukkanen J. Long-term effects of ovariectomy on the mechanical properties and chemical composition of rat bone. *Bone* 1997;20:207-212.
22. Heine PA, Taylor JA, Iwamoto GA, Lubahn DB, Cooke PS. Increased adipose tissue in male and female estrogen receptor-alpha knockout mice. *Proc Natl Acad Sci U S A* 2000;97:12729-12734.
23. Parfitt AM, Drezner MK, Glorieux FH, et al. Bone histomorphometry: standardization of nomenclature, symbols, and units. Report

- of the ASBMR Histomorphometry Nomenclature Committee. *J Bone Miner Res* 1987;2:595-610.
24. Wronski TJ, Cintron M, Dann LM. Temporal relationship between bone loss and increased bone turnover in ovariectomized rats. *Calcif Tissue Int* 1988;43:179-183.
 25. Wronski TJ, Dann LM, Horner SL. Time course of vertebral osteopenia in ovariectomized rats. *Bone* 1989;10:295-301.
 26. Li M, Shen Y, Wronski TJ. Time course of femoral neck osteopenia in ovariectomized rats. *Bone* 1997;20:55-61.
 27. Marshall D, Johnell O, Wedel H. Meta-analysis of how well measures of bone mineral density predict occurrence of osteoporotic fractures. *BMJ* 1996;312:1254-1259.
 28. Riggs BL, Melton LJ 3rd. Bone turnover matters: the raloxifene treatment paradox of dramatic decreases in vertebral fractures without commensurate increases in bone density. *J Bone Miner Res* 2002;17:11-14.
 29. Ke HZ, Jee WS, Zeng QQ, Li M, Lin BY. Prostaglandin E2 increased rat cortical bone mass when administered immediately following ovariectomy. *Bone Miner* 1993;21:189-201.
 30. Brouwers JE, van Rietbergen B, Huiskes R, Ito K. Effects of PTH treatment on tibial bone of ovariectomized rats assessed by in vivo micro-CT. *Osteoporos Int* 2009;20:1823-1835.
 31. Samnegard E, Iwaniec UT, Cullen DM, Kimmel DB, Recker RR. Maintenance of cortical bone in human parathyroid hormone (1-84)-treated ovariectomized rats. *Bone* 2001;28:251-260.
 32. Li M, Shen Y, Qi H, Wronski TJ. Comparative study of skeletal response to estrogen depletion at red and yellow marrow sites in rats. *Anat Rec* 1996;245:472-480.
 33. Comelekoglu U, Bagis S, Yalin S, et al. Biomechanical evaluation in osteoporosis: ovariectomized rat model. *Clin Rheumatol* 2007;26:380-384.
 34. Luhach I, Idiyatullin D, Lynch CC, et al. Rapid ex vivo imaging of P4III prostate to bone tumor with SWIFT-MRI. *Magn Reson Med* 2014;72:858-863.
 35. Rautiainen J, Lehto LJ, Tiitu V, et al. Osteochondral repair: evaluation with sweep imaging with fourier transform in an equine model. *Radiology* 2013;269:113-121.
 36. Weiger M, Brunner DO, Dietrich BE, Muller CF, Pruessmann KP. ZTE imaging in humans. *Magn Reson Med* 2013;70:328-332.
 37. Weiger M, Pruessmann KP, Hennel F. MRI with zero echo time: hard versus sweep pulse excitation. *Magn Reson Med* 2011;66:379-389.